Active subspace uncertainty quantification for a polydomain ferroelectric phase-field model

Lider S. Leon, Ralph C. Smith, Paul Miles, William S. Oates

Lider S. Leon, Ralph C. Smith, Paul Miles, William S. Oates, "Active subspace uncertainty quantification for a polydomain ferroelectric phase-field model," Proc. SPIE 10596, Behavior and Mechanics of Multifunctional Materials and Composites XII, 105960T (22 March 2018); doi: 10.1117/12.2297207

SPIE.

Event: SPIE Smart Structures and Materials + Nondestructive Evaluation and Health Monitoring, 2018, Denver, Colorado, United States

Active Subspace Uncertainty Quantification for a Polydomain Ferroelectric Phase-Field Model

Lider S. Leon[a], Ralph C. Smith[a], Paul Miles[a], and William S. Oates[b]

[a]Department of Mathematics, North Carolina State University, Raleigh, NC 27695
[b]Florida Center for Advanced Aero Propulsion (FCAAP), Department of Mechanical Engineering, Florida A & M and Florida State University, Tallahassee, FL 32310

ABSTRACT

Quantum-informed ferroelectric phase field models capable of predicting material behavior, are necessary for facilitating the development and production of many adaptive structures and intelligent systems. Uncertainty is present in these models, given the quantum scale at which calculations take place. A necessary analysis is to determine how the uncertainty in the response can be attributed to the uncertainty in the model inputs or parameters. A second analysis is to identify *active subspaces* within the original parameter space, which quantify directions in which the model response varies most dominantly, thus reducing sampling effort and computational cost. In this investigation, we identify an active subspace for a poly-domain ferroelectric phase-field model. Using the active variables as our independent variables, we then construct a surrogate model and perform Bayesian inference. Once we quantify the uncertainties in the active variables, we obtain uncertainties for the original parameters via an inverse mapping. The analysis provides insight into how active subspace methodologies can be used to reduce computational power needed to perform Bayesian inference on model parameters informed by experimental or simulated data.

Keywords: Ferroelectric materials, ferroelectricity, active subspaces, surrogate model, uncertainty quantification, Bayesian inference

1. INTRODUCTION

Ferroelectric materials are widely employed in a variety of engineering applications due to their electromechanical properties. Some of these applications include flow control transducers, energy harvesting circuits, and flying microrobots.[5,12,15] The modest power requirements, nanometer positioning accuracy and solid state nature make ferroelectric materials ideal for these types of applications. This motivates the need for accurate prediction of material behavior, ranging in scales from the material's atomic configuration to a macroscopic continuum domain.

Quantum-scale density functional theory (DFT) calculations are performed to accurately estimate many structure-dependent properties in the materials. Nonetheless, DFT calculations are not feasible when solving problems on a continuum scale. This requires the introduction of phase-field models, characterizing polarization and strain order parameters to simulate larger scale domain structure evolution.

The uncertainty in data and the introduction of the order parameters, which homogenizes effects from the atomic structure, leads to uncertainty in the phase-field models, which can be quantified via the use of Bayesian statistical methods. These methods may be computationally expensive to implement depending on the model evaluation cost and/or the number of unknown model inputs and associated uncertainties. The uncertainty and cost are increased when considering effects across the multi-domain structure of ferroelectric materials.

Further author information: (Send correspondence to Lider S. Leon.)
Lider S. Leon: E-mail: lsleon@ncsu.edu,
Ralph C. Smith: E-mail: rsmith@ncsu.edu
William S. Oates: E-mail: woates@fsu.edu
Paul Miles: E-mail: pmilescs@gmail.com

Behavior and Mechanics of Multifunctional Materials and Composites XII,
edited by Hani E. Naguib, Proc. of SPIE Vol. 10596, 105960T · © 2018 SPIE
CCC code: 0277-786X/18/$18 · doi: 10.1117/12.2297207

Subset selection methods such as global sensitivity analysis, isolate parameters that are most influential or contribute the most to a model's output as well as those having minimal influence. Ideally, the parameter dimension is reduced such that model calibration and uncertainty quantification is more feasible.

Subspace selection methods provide an alternative appealing approach in that they identify important directions in the full parameter space affecting the output the most. We refer to these methods as *active subspace* methods since *active variables* are determined as weighted linear combinations of the parameters indicating directions of strongest variability. These directions are separated from ones in which the model response is relatively flat, yielding the *inactive* variables.

In this investigation we consider a 180° polydomain phase-field energy model for lead titanate. The phase-field energy model is composed of a stored energy, as a function of elastic, Landau or polarization, electrostrictive, and polydomain gradient energy relations. We are interested in the uncertainty and influence of all the unknown parameters except for the elastic coefficients. The elastic coefficient properties influencing the mechanical energy for lead titanate are well-known from other investigations,[4] and are therefore fixed in our analysis.

We determine an active subspace for the parameters via the use of gradient approximation methods, ranking the most important directions in the space of all inputs. We then use this active subspace to construct a response surface as a function of the active variables which approximates the original model output response. Finally, we implement Bayesian analysis techniques along with our response surface to infer the distributions of the model parameters.

This paper is divided into the following sections. The next section introduces the model governing equations including the mondomain and 180° domain wall relations. We present the active subspace and Bayesian inference methodologies in Section 3, whereas results are presented in Section 4. Lastly, Section 5 provides concluding remarks.

2. MODEL

Consider the stored energy model

$$u = u_M(\varepsilon_{ij}) + u_P(P_i) + u_G(P_{i,j}) + u_C(\varepsilon_{ij}, P_i),\ i,j = 1,2,3, \tag{1}$$

where

$$\begin{aligned}
u_M &= \frac{c_{11}}{2}\left(\varepsilon_{11}^2+\varepsilon_{22}^2+\varepsilon_{33}^2\right) + c_{12}\left(\varepsilon_{11}\varepsilon_{22}+\varepsilon_{22}\varepsilon_{33}+\varepsilon_{11}\varepsilon_{33}\right) + 2c_{44}\left(\varepsilon_{12}^2+\varepsilon_{23}^2+\varepsilon_{13}^2\right),\\
u_P &= \alpha_1(P_1^2+P_2^2+P_3^2) + \alpha_{11}(P_1^2+P_2^2+P_3^2)^2 + \alpha_{12}(P_1^2P_2^2+P_2^2P_3^2+P_1^2P_3^2) + \alpha_{111}(P_1^6+P_2^6+P_3^6)\\
&\quad +\alpha_{112}\left[P_1^4(P_2^2+P_3^2)+P_2^4(P_1^2+P_3^2)+P_3^4(P_1^2+P_2^2)\right] + \alpha_{123}P_1^2P_2^2P_3^2\\
u_C &= -q_{11}\left(\varepsilon_{11}P_1^2+\varepsilon_{22}P_2^2+\varepsilon_{33}P_3^2\right) - q_{12}\left[\varepsilon_{11}\left(P_2^2+P_3^2\right)+\varepsilon_{22}\left(P_1^2+P_3^2\right)+\varepsilon_{33}\left(P_1^2+P_2^2\right)\right]\\
&\quad -q_{44}\left(\varepsilon_{12}P_1P_2+\varepsilon_{13}P_1P_2+\varepsilon_{23}P_2P_3\right),\\
u_G &= \frac{g_{11}}{2}\left(P_{1,1}^2+P_{2,2}^2+P_{3,3}^2\right) + g_{12}\left(P_{1,1}P_{2,2}+P_{1,1}P_{3,3}+P_{2,2}P_{3,3}\right)\\
&\quad +\frac{g_{44}}{2}\left[\left(P_{1,2}+P_{2,1}\right)^2+\left(P_{1,3}+P_{3,1}\right)^2+\left(P_{2,3}+P_{3,2}\right)^2\right].
\end{aligned}$$

Here, u_M, u_P, u_C and u_G are the mechanical energy, Landau or polarization energy, electrostrictive energy and gradient energy respectively, as described by Cao and Cross.[1] In the relations, the unknown parameters c_{11}, c_{12} and c_{44} are the elastic coefficients, q_{11}, q_{12}, and q_{44} are the electrostrictive coefficients, $\alpha_1, \alpha_{11}, \alpha_{12}, \alpha_{111}$, and α_{112} are the Landau phenomenological parameters, and g_{11}, g_{12} and g_{44} are the gradient energy exchange parameters. The conditions for static equilibrium, for polarization $\mathbf{P}$ and strain $\boldsymbol{\varepsilon}$ are

$$\frac{\partial}{\partial x_j}\left(\frac{\partial u}{\partial P_{i,j}}\right) - \frac{\partial u}{\partial P_i} = 0, \quad (i,j = 1,2,3), \tag{2}$$

$$\sigma_{ij,j}^{\text{tot}} = \frac{\partial}{\partial x_j}\left(\frac{\partial u}{\partial \varepsilon_{ij}}\right) = 0. \tag{3}$$

We employ the equilibrium conditions in the monodomain and polydomain structures.

2.1 Mondomain Energy

In the case of monodomain structures, or regions of uniformly oriented polarization, the stored energy is described by the mechanical, Landau, and electrostrictive energy relations. This uniformity and the equilibrium conditions (2)-(3), yield the spontaneous polarization and strain

$$P_3 = P_0 = \left(\frac{-\alpha'_{11} + (\alpha'^2_{11} - 3\alpha_1\alpha_{111})^{1/2}}{3\alpha_{111}}\right)^{1/2}, \tag{4}$$

$$\begin{aligned} \varepsilon_{11} = \varepsilon_{22} = \varepsilon_{\perp} &= \frac{P_0^2}{3}\left(\frac{\hat{q}_{11}}{\hat{c}_{11}} - \frac{\hat{q}_{22}}{\hat{c}_{22}}\right), \\ \varepsilon_{33} = \varepsilon_{||} &= \frac{P_0^2}{3}\left(\frac{\hat{q}_{11}}{\hat{c}_{11}} + \frac{2\hat{q}_{22}}{\hat{c}_{22}}\right), \end{aligned} \tag{5}$$

where

$$\begin{aligned} \alpha'_{11} &= \alpha_{11} + \frac{4c_{12}q_{11}q_{12} - q_{11}^2(c_{11}+c_{12}) - 2c_{11}q_{12}^2}{2\hat{c}_{11}\hat{c}_{22}}, \\ \hat{c}_{11} &= c_{11} + 2c_{12}, \\ \hat{c}_{22} &= c_{11} - c_{12}, \\ \hat{q}_{11} &= q_{11} + 2q_{12}, \\ \hat{q}_{22} &= q_{11} - q_{12}, \\ \alpha_1^+ &= \alpha_1 - q_{11}\varepsilon_{33} - q_{12}(\varepsilon_{11} + \varepsilon_{22}). \end{aligned} \tag{6}$$

We obtain the monodomain energy density u_0 by substituting the polarization (4) and strain (5) into the stored energy equation (1).

2.2 180° Domain Wall Model

The 180° domain walls separate domains in which polarization is oriented in opposite directions. We assume the polarization vector to be

$$\mathbf{P} = (0, 0, P_3(x_1)). \tag{7}$$

Away from the domain wall, the material exhibits spontaneous polarization such that we obtain the boundary conditions

$$\begin{aligned} &\lim_{x_1\to\pm\infty} \mathbf{P} = (0, 0, \pm P_0), \\ &\lim_{x_1\to\pm\infty} \sigma_{ij}^{\text{tot}}(x_1) = 0, \quad ij = 11, 22, 33, \\ &\lim_{x_1\to\pm\infty} \sigma_{ij}^{\text{tot}}(x_1) = 0, \quad ij = 23, 13, 12. \end{aligned} \tag{8}$$

Employing the static equilibrium condition (2) yields the differential equation

$$\left(\frac{\partial u}{\partial P_{3,1}}\right)_1 - \frac{\partial u}{\partial P_3} = 0 \implies 2\alpha_1^+ P_3 + 4\alpha_{11} P_3^3 + 6\alpha_{111} P_3^5 - g_{44} P_{3,11} = 0, \tag{9}$$

where

$$\alpha_1^+ = \alpha_1 - q_{11}\varepsilon_{33} - q_{12}(\varepsilon_{11} + \varepsilon_{22}).$$

The conditions (3) and (8) also yields the differential equation

$$\sigma_{11,1} = 0 = c_{11}\varepsilon_{11,1} + c_{12}(\varepsilon_{22,1} + \varepsilon_{33,1}) - 2q_{12}P_3 P_{3,1}. \tag{10}$$

We employ the finite-difference method presented the work by Miles et al.[7] to obtain a solution for polarization $P_3(x_1)$ and strain $\varepsilon_{11}(x_1)$. Substituting solutions for polarization and strain into (1), we obtain the energy surface u_{180} quantifying domain wall effects. The total energy associated with the 180 degree domain wall is thus quantified by taking the difference between u_{180} and the monodomain energy u_0, and integrating through the x_1 density. This yields the relation

$$E_{180^\circ}(\theta_{180}) = \int_{-\infty}^{\infty} (u_{180} - u_0) dx_1, \tag{11}$$

where

$$\theta_{180} = [\alpha_1, \alpha_{11}, \alpha_{111}, q_{11}, q_{12}, g_{44}]. \tag{12}$$

Here, θ_{180} represents the unknown parameters.

3. ACTIVE SUBSPACE AND BAYESIAN INFERENCE

3.1 Active Subspace

We define the active subspace for a scalar quantity of interest with respect to some parameters following the derivation presented by Leon et al.[6] Given $Y = f(\Theta)$, we compute the matrix

$$\mathbf{C} = \mathbb{E}\left[(\nabla_\theta f)(\nabla_\theta f)^T\right]. \tag{13}$$

The matrix $\mathbf{C}$ is symmetric and positive definite by construction. Thus, it has the real eigenvalue decomposition

$$\mathbf{C} = \mathbf{W}\Lambda\mathbf{W}^T,$$

for $\Lambda = \mathrm{diag}(\lambda_1, \lambda_2, \ldots, \lambda_p)$, $\lambda_1 \geq \cdots \geq 0$. Based on a possible gap in the eigenvalue spectrum, we consider the partitions $\mathbf{W} = [\mathbf{W}_1, \mathbf{W}_2]$ and

$$\Lambda = \begin{bmatrix} \Lambda_1 & \\ & \Lambda_2 \end{bmatrix}, \quad \Lambda_1 = \mathrm{diag}(\lambda_1, \ldots, \lambda_m), \quad m < p.$$

Using this significant gap, we define the new rotated coordinate variables

$$\mathbf{y} = \mathbf{W}_1^T\theta, \quad \mathbf{z} = \mathbf{W}_2^T\theta,$$

where $\mathbf{y} \in \mathbb{R}^m$ and $\mathbf{z} \in \mathbb{R}^{p-m}$. Based on this transformation, on average the output f varies more dominantly due to variability and perturbations in the directions dictated by $\mathbf{y}$, than in the directions dictated by $\mathbf{z}$,[14] defining the active and inactive subspaces.

In practice, construction of the matrix (13) may require computing high dimensional integrals. Therefore, based on Constantine[14] and Bang,[13] we approximate the gradient matrix

$$\mathbf{G} = \frac{1}{\sqrt{M}} \left[\nabla_\theta f_1 \quad \nabla_\theta f_2 \quad \cdots \quad \nabla_\theta f_M \right].$$

composed of gradient, or approximate gradient evaluations at values in the original input space. We then use the singular value decomposition (SVD) to extract an input active subspace basis. The basis for the active subspace is contained in the matrix of singular vectors $\mathbf{U}$ in

$$\mathbf{G} = \mathbf{U}\Sigma\mathbf{V}^T. \tag{14}$$

Note that the diagonal matrix Σ contains the squared roots of the eigenvalues of $\mathbf{C}$. This methodology for computing the active subspace is equivalent to the methodology employed by the formation of the matrix $\mathbf{C}$ as shown by Russi.[10]

3.2 Scaling Maps

Note that for the construction of the active subspace and response surface, we consider two cases for the parameter distributions.

In the first case, we consider the parameters to be uniformly distributed such that

$$\Theta_i \sim \mathcal{U}(\theta_i^{nom} - \delta|\theta_i^{nom}|, \theta_i^{nom} + \delta|\theta_i^{nom}|). \tag{15}$$

Here, θ_i^{nom}, $i = 1, \ldots, p$, represents nominal values of the parameters θ. For this analysis, we choose $\delta = 0.10$. To avoid scaling issues due to the differences in units of magnitudes for different sets of parameters, we scale all the intervals in the uniform distribution to the interval [0,1]. The scaling normalizes all inputs, while removing units and ensuring that parameters containing relatively large values do not affect the analysis disproportionally. To scale back to the natural input values for the model evaluations, we use the mapping

$$\theta = U_{map}(\mathbf{x}) = \text{diag}(\vec{\theta}_u - \vec{\theta}_\ell)\mathbf{x} + \vec{\theta}_\ell, \tag{16}$$

where $\mathbf{x}$ is a p-vector with values between 0 and 1, and $\vec{\theta}_\ell$ and $\vec{\theta}_u$ are the vectors with the lower and upper bounds of the parameters θ. Note that in our problem, the upper and lower bound vectors are

$$\vec{\theta}_\ell = \theta^{nom} - \delta|\theta^{nom}| \text{ and } \vec{\theta}_u = \theta^{nom} + \delta|\theta^{nom}|,$$

where θ^{nom} is the vector of nominal values for the parameters.

In the second case, we consider the parameters to be normally distributed,

$$\Theta \sim \mathcal{N}(\theta^{nom}, \mathbf{V}), \tag{17}$$

where $\mathbf{V}$ is the covariance matrix defined by

$$\mathbf{V} = \begin{bmatrix} \sigma_1^2 & \text{cov}(\Theta_1, \Theta_2) & \cdots & \text{cov}(\Theta_1, \Theta_p) \\ \text{cov}(\Theta_2, \Theta_1) & \sigma_2^2 & \cdots & \\ \vdots & \vdots & \ddots & \\ \text{cov}(\Theta_p, \Theta_1) & & & \sigma_p^2 \end{bmatrix}.$$

Similar to the uniform distribution, we normalize all inputs to avoid discrepancies in the analysis due to parameters with relatively large values and units of magnitude. We use a Cholesky decomposition of $\mathbf{V}$, where

$$\mathbf{V} = \mathbf{A}\mathbf{A}^T,$$

such that the mapping to the natural input values for model evaluations is

$$\theta = N_{map}(\mathbf{x}) = \theta^{nom} + \mathbf{A}\mathbf{x}. \tag{18}$$

Here, $\mathbf{x}$ are generated from the standard normal distribution $\mathcal{N}(\mathbf{0}, \mathbf{I})$.

3.3 Gradient Evaluations

Using the maps defined in the previous section, we now introduce transformed gradients which account for the normalization of the input parameters. Since the simulations of the physical model require the natural model input values, we present a methodology where we evaluate the gradient in the normalized space to avoid discrepancies due to different units of magnitude. We again consider the two scenarios of uniformly distributed and normally distributed parameters. To implement the gradient evaluations in the uniform normalized space, we let $\mathbf{T}_U = \text{diag}(\vec{\theta}_u - \vec{\theta}_\ell)$, and define the function

$$g(\mathbf{x}) = f(\mathbf{T}_U\mathbf{x} + \vec{\theta}_\ell) = f(\theta). \tag{19}$$

We then use this function to determine an appropriate gradient defined as

$$\begin{aligned} \frac{g(\mathbf{x}+\Delta) - g(\mathbf{x})}{\Delta} &= \frac{f(\mathbf{T}_U(\mathbf{x}+\Delta) + \vec{\theta}_\ell) - f(\mathbf{T}_U\mathbf{x} + \vec{\theta}_\ell)}{\Delta} \\ &= \frac{f(\mathbf{T}_U\mathbf{x} + \vec{\theta}_\ell + \mathbf{T}_U\Delta) - f(\mathbf{T}_U\mathbf{x} + \vec{\theta}_\ell)}{\Delta} \\ &= \frac{f(\theta + \mathbf{T}_U\Delta) - f(\theta)}{\Delta}, \end{aligned} \tag{20}$$

where the last equality follows from (16). This transformed gradient avoids discrepancies, like cancellation errors or inaccurate results due to different orders of magnitude in the parameters. We implement the gradient (20) for the determination of the active subspace when considering the parameters to be uniformly distributed.

Similarly, when the parameters are normally distributed, we define

$$h(\mathbf{x}) = f(\mathbf{A}\mathbf{x} + \theta^{nom}) = f(\theta), \tag{21}$$

such that the normalized gradient is

$$\begin{aligned} \frac{h(\mathbf{x}+\Delta) - h(\mathbf{x})}{\Delta} &= \frac{f(\mathbf{A}(\mathbf{x}+\Delta) + \theta^{nom}) - f(\mathbf{A}\mathbf{x} + \theta^{nom})}{\Delta} \\ &= \frac{f(\theta + \mathbf{A}\Delta) - f(\theta)}{\Delta}. \end{aligned} \tag{22}$$

This gradient is used when determining the active subspace assuming parameters to be normally distributed.

Using these derivative terms, we then implement the Morris finite-difference[9] approach to approximate the gradient matrix $\mathbf{G}$ of Section 3.1. The main idea is to first select normalized initial vectors $\mathbf{x}^j \in \mathbb{R}^p$, $j = 1, \ldots, M$, sampled from a probability density $\rho(\mathbf{x})$. In our case, we take $\rho(\mathbf{x})$ to be the uniform distribution from (15), and the normal distribution from (17). We then construct a set of coarse derivative approximations termed elementary effects,

$$d_i(\mathbf{x}^j) = \frac{g(x_1^j, \ldots, x_{i-1}^j, x_i^j + \Delta, x_{i+1}^j, \ldots, x_p^j) - g(\mathbf{x}^j)}{\Delta} = \frac{g(\mathbf{x}^j + \Delta \cdot \mathbf{e}_i) - g(\mathbf{x}^j)}{\Delta},$$

given a step size Δ, for the i^{th} parameter and j^{th} sample point drawn from $\rho(\mathbf{x})$. We use this method, as presented in Algorithm 3.1, to construct the columns of the gradient matrix for the active subspace construction.

3.4 Response Surface

Response surfaces are constructed to approximate the original function output. We use Algorithm 3.2 to construct the response surface via the function $r(\mathbf{y})$. Next, we show how the response surface is used in conjunction with the active subspace to reduce the computational cost, otherwise required by Bayesian inference in the original input space.

Algorithm 3.1: Morris finite-difference method gradient approximation.[9]

(0) Identify the number of desired columns M, appropriate step size Δ, and probability density $\rho(\mathbf{x})$. Use the model function $g(\mathbf{x})$ or $h(\mathbf{x})$ depending on the probability density $\rho(\mathbf{x})$.

for $j = 1, \ldots, M$

(1) Construct the row vector $\mathbf{D}_{1\times p}$ with randomly chosen entries $\pm\Delta$, where Δ is the step size.

(2) Select $\mathbf{x}^j$ from the probability density $\rho(\mathbf{x})$. In our case this is the uniform or normal distribution. Evaluate the model function at the sampled value along with the elementary effect as follows.
for $i = 1, \ldots, p$
$d_i = \frac{g(\mathbf{x}_i^j + \mathbf{D}(i)\cdot\mathbf{e}_i) - g(\mathbf{x}^j)}{\mathbf{D}(i)}$, where $\mathbf{e}_i$ is the i^{th} standard basis vector.
end

(3) Let $\hat{\mathbf{G}}(:, j) = \mathbf{d}$, where $\hat{\mathbf{G}}$ is the gradient matrix approximation.

end

Algorithm 3.2: Algorithm for constructing response surface based on active subspace.

(0) Sample the training input values $\mathbf{x}_i$ with respect to its probability density function and construct corresponding responses $q_i = g(\mathbf{x}_i)$.

(1) Project the sampled values $\mathbf{x}_i$ onto the active subspace by using the transformation $\mathbf{y} = \mathbf{W}_1^T\mathbf{x}_i$.

(2) Using regression analysis construct a response surface $r(\mathbf{y})$, using q_i, such that $q_i \approx r(\mathbf{y}_i)$.

(3) Verify the response surface by approximating the original function $g(\mathbf{x}) \approx r(\mathbf{W}_1^T\mathbf{x})$.

3.5 Bayesian Inference

We use the response surface to perform Bayesian inference on the active subspace. In this investigation we employ Gaussian prior distributions, which avoid the issues associated with rotating hypercubes in uniform distributions, resulting in marginal and conditional distributions which are not uniform.[14] Extending active subspace Bayesian inference to general prior distributions constitutes future work. To employ Bayesian inference for constructing marginal and multivariate posterior distributions, we use the Delayed Adaptive Metropolis Algorithm (DRAM) described in detail by Haario[3] and Smith.[11] Algorithm 3.3 presents the framework we implement in this investigation.

Algorithm 3.3: Algorithm for performing Bayesian inference on active subspace.

(1) Determine an appropriate Gaussian prior distribution for the active variable $\mathbf{y}$ based on the projection of the parameters $\mathbf{x}$ onto the active subspace.

(2) Employ DRAM to calibrate the active variables $\mathbf{y}$.

(3) Transform the resulting chain of accepted active variable samples into the full normalized space via the relation

$$\mathbf{x}^k = \mathbf{U}(:, 1:n)\mathbf{y}^k + \mathbf{U}(:, n+1:p)\mathbf{z}^k,$$

where $k = 1, \ldots K$, $K \equiv$ the number of samples in the chain obtained from DRAM. Here, $\mathbf{z}^k$ denotes the inactive variables, which are sampled from an appropriate prior distribution determined based on the projection from the original input space.

4. RESULTS

4.1 Active Subspace Bayesian Inference

The gradient matrix for the active subspace is constructed following the methodology in Section 3.1. Note that the values for θ_{180} are sampled based on a uniform distribution such that

$$\Theta_i \sim \mathcal{U}(\theta_i^{nom} - 0.10|\theta_i^{nom}|, \theta_i^{nom} + 0.10|\theta_i|),$$

where the absolute values $|\theta_i^{nom}|$, $i = 1, \ldots, 6$, for nominal values of θ_{180} are obtained from Miles et. al.[7] We compare the results of this sampling distribution with one where the parameters are normally distributed such that

$$\Theta_{180} \sim \mathcal{N}(\theta^{nom}, \mathbf{V}), \tag{23}$$

where θ^{nom} is the vector of nominal values for θ_{180}. To accommodate the possible correlation structure between the parameters we first select a prior original space covariance matrix

$$\mathbf{V}_{or} = \text{diag}\Big[(0.10|\theta_1^{nom}|)^2, (0.10|\theta_2^{nom}|)^2, \ldots, (0.10|\theta_6^{nom}|)^2\Big]$$

to use the scaling map defined in Section 3.2. We then employ DRAM to calibrate the model (11) with respect to 500 synthetic data points generated from perturbed evaluations of θ^{nom}. This analysis yields the sampling normalized covariance matrix

$$\mathbf{V} = \begin{bmatrix} 0.9448 & -0.0036 & 0.0880 & 0.1385 & 0.0155 & -0.0463 \\ -0.0036 & 0.7872 & 0.0320 & 0.3901 & 0.0449 & -0.0175 \\ 0.0880 & 0.0320 & 0.9414 & 0.0743 & -0.0464 & 0.0622 \\ 0.1385 & 0.3901 & 0.0743 & 0.2245 & 0.0817 & -0.0667 \\ 0.0155 & 0.0449 & -0.0464 & 0.0817 & 0.9539 & 0.0824 \\ -0.0463 & -0.0175 & 0.0622 & -0.0667 & 0.0824 & 0.8805 \end{bmatrix}. \tag{24}$$

We present the results of the singular value decomposition from the gradient matrix approximation $\hat{\mathbf{G}}$ for (11), considering both sampling distributions for θ_{180}, in Figure 1(a). Based on the gap between the first and second singular values, we take the dimension of the active subspace to be equal to 1. In Figure 1(b) we present the activity scores for a one-dimensional active subspace. These results indicate that the parameters α_{11} and q_{11} are most sensitive. Therefore, in anticipation of the Bayesian inference on the active subspace, results should indicate that these parameters are most informed as a result of the analysis.

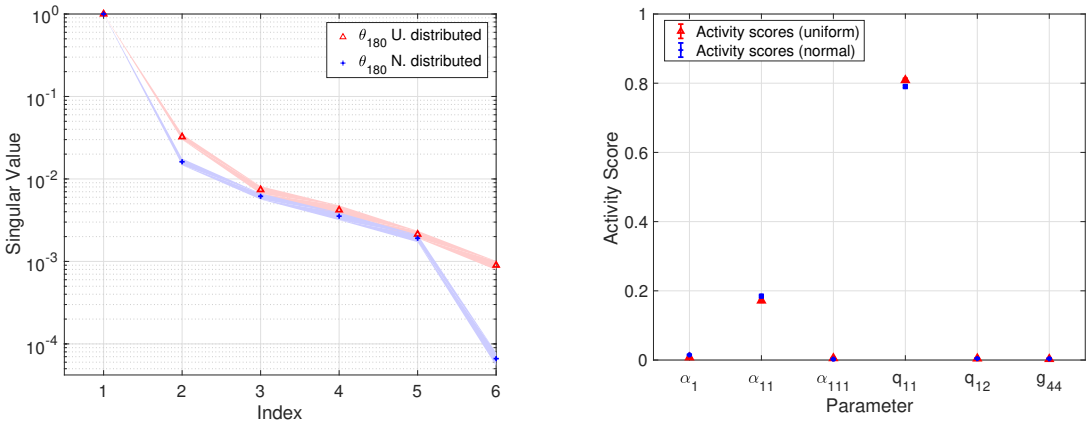

(a) (b)

Figure 1. Comparison of the (a) singular values and (b) activity scores obtained from the gradient matrix $\mathbf{G}$ for (11), constructed using uniformly and uncorrelated normally distributed parameters.

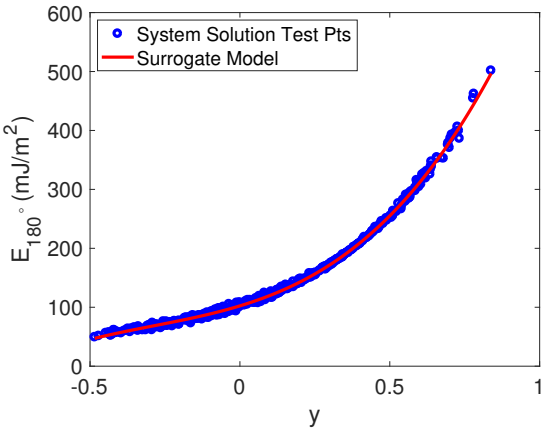

Figure 2. Response surface obtained from the active subspace for (11).

Dimension	1	2	3	4	5
MRE	0.0194	0.0036	0.0028	0.0014	7.8669e-4

Table 1. Mean relative errors (MRE) computed for response surfaces constructed based on different possible dimensions of the active subspace.

Next, we construct the response surface for (11). We implement Algorithm 3.2 to obtain the response surface. Note that we use multivariate polynomial regression in the implementation of the algorithm. We present the response surface fit to the original function in Figure 2. To validate the fit of our response surface, we present the mean relative errors (MRE) obtained for different possible dimensions for the active subspace, in Table 1

We now employ the response surface in the active subspace Bayesian inference. Note that the prior distributions were built as Gaussian distributions about the nominal values from Miles.[7] The priors were taken to be

$$\Theta_{180} \sim \mathcal{N}(\theta^{nom}, \mathbf{V}_{pr})$$

where $\mathbf{V}_{pr} = \text{diag}\Big[(0.20|\theta_1^{nom}|)^2, (0.20|\theta_2^{nom}|)^2, \ldots, (0.20|\theta_6^{nom}|)^2\Big]$.

We implement Algorithm 3.3 for the active subspace of (11). In the analysis, we used the numerical implementation of Miles et. al,[7] to generate synthetic data with perturbed evaluations of the nominal values θ^{nom}. We used 500 synthetic data points to inform our response surface. The results with the prior and posterior distributions are presented in Figure 3. Additionally, we present the pairwise density plots in Figure 4.

The distributions for parameters $\alpha_1, \alpha_{111}, q_{12}$ and g_{44} change minimally with respect to the prior distributions. The results imply that the parameters being informed by the Bayesian inference are those whose directions are more dominant with respect to the active subspace, as indicated by Figure 1. This is explained due to the coupling of the parameters in the solution of the differential equation (9). Note also that the results for the pairwise correlation plots are in agreement with both the derived covariance matrix (24) and the active subspace results.

5. CONCLUDING REMARKS

We performed an active subspace analysis on a phase-field energy model for polydomain lead titanate crystals. Next, we constructed a response surface which approximated the original model response, only as a function of the active variables. The determination of the response surface reduced the cost in the model evaluation, which otherwise requires a numerical finite difference implementation.[7] Finally, we employed the active subspace response surface to obtain posterior distributions for the model parameters via the use of the DRAM algorithm.

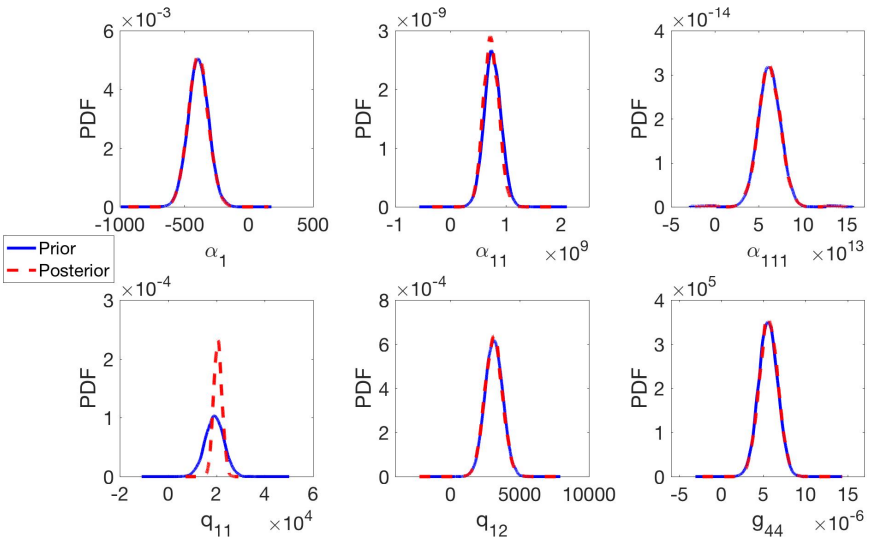

Figure 3. Comparison of prior and posterior densities for θ_{180} after the implementation of Algorithm 3.3.

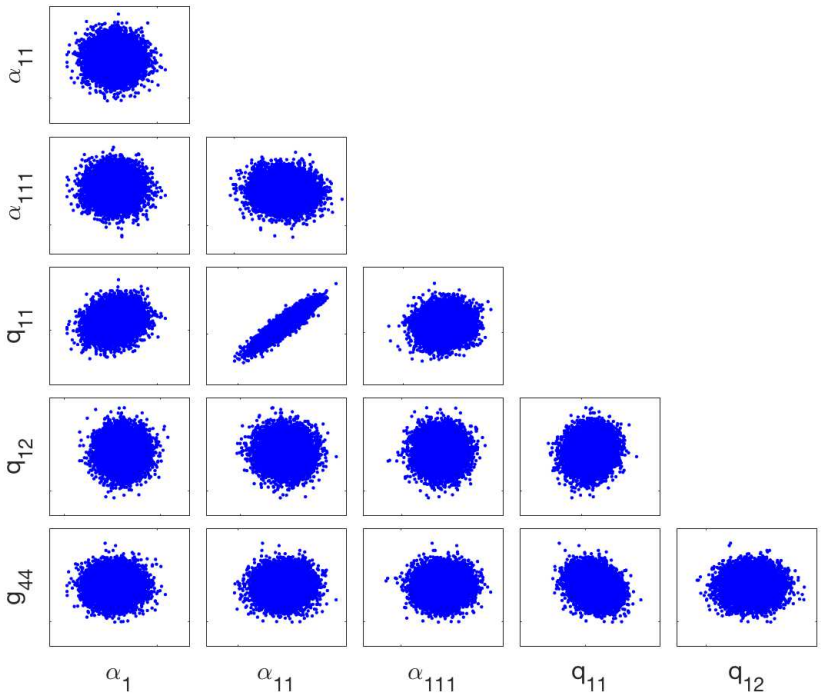

Figure 4. Pairwise density plots for θ_{180} after the implementation of Algorithm 3.3.

In addition to mechanical energy, electrostrictive energy, and Landau energy relations, the polydomain energy model entails the consideration of the gradient energy which governs interactions across 180° domain walls. It is observed that contributions from the coupling of the model parameters in the differential equation (9) have an effect on the total energy associated with the domain wall. In future work, we will consider combined effects on the total energy due to the interactions across both 180° and 90° domain walls. This will involve a rotation of

the order parameters $\mathbf{P}$ and ε along the 90° domain wall, in order to facilitate the analysis. We will also compare our active subspace Bayesian inference results with results obtained by employing our inference methods on the full parameter space.

ACKNOWLEDGMENTS

This material is based upon work supported by the National Science Foundation under Grant No. DGE-1633587. The research of LL and RCS was also supported in part by the NSF Grant CMMI-1306290 Collaborative Research CDS&E, whereas the research of PM and WSO was supported in part by the NSF Grant CMMI-1306320 Collaborative Research CDS&E.

REFERENCES

[1] Cao, W. and Cross, L., "Theory of tetragonal twin structures in ferroelectric perovskites with a first-order phase transition," *Phys. Rev. B* **44**(1), 5-12 (1991).

[2] Falk, F., "Ginzburg-Landau theory of static domain walls in shape-memory alloys". *Zeitschrift fur Physik B Condensed Matter*, **51**(2), pp. 177-185 (1983).

[3] Haario, H., Laine, H., Mira, A., and Saksman, E., "DRAM: Efficient adaptive MCMC," *Stat Comput*, **16**, 339-354 (2006).

[4] King-Smith, R., and Vanderbilt, D., "First-principles investigations of ferroelectricity in perovskite compounds," *Phys. Rev. B* **49**, 5828-5844 (1994).

[5] Kumar, V., Hays, M., Fernandez, E., Oates, W., and Alvi, F.S., "Flow sensitive actuators for micro-air vehicles". *Smart Materials and Structures*, 20: 105033 (2011).

[6] Leon, L,, Miles, P., Smith, R., and Oates, W., "Identifiability and active subspace analysis for a polydomain ferroelectric phase-field model," *Proceedings of the SMASIS 2017 Conference*, Snowbird, UT (2017).

[7] Miles, P., Oates, W., Leon, L., and Smith, R.C., "Uncertainty analysis of ferroelectric polydomain structures," *Proceedings of the SMASIS 2017 Conference*, Snowbird, UT (2017).

[8] Miles, P., Oates, W., Leon, L. and Smith, R.C., "Analysis of a multi-axial quantum-informed ferroelectric continuum model: Part 1 - uncertainty quantification," *Journal of Intelligent Material Systems and Structures*, Submitted (2017).

[9] Morris, M.D., "Factorial sampling plans for preliminary computational experiments," *Technometrics*, **33**(2), pp. 161-174, 1991.

[10] Russi,T.M., "Uncertainty quantification with experimental data and complex system models," PhD thesis, UC Berkeley, 2010.

[11] Smith, R. C., [*Uncertainty Quantification: Theory, Implementation and Applications*], SIAM, Philadelphia, PA (2014).

[12] Song, H.J., Choi, Y.T., Wereley, N.M. and Purekar, A.S., "Energy harvesting devices using macro-fiber composite materials," *Journal of Intelligent Material Systems and Structures* **21**(6): 647-658 (2010).

[13] Bang, Y., Abdel-Khalik, H. S., and Hite, J. M., "Hybrid reduced order modeling applied to nonlinear models," *International Journal for Numerical Methods in Engineering* **91**, 929-949 (2012).

[14] Constantine, P. G., [*Active Subspaces: Emerging Ideas for Dimension Reduction in Parameter Studies*], SIAM, Philadelphia, PA (2015).

[15] Wood, R.J., "The first takeoff of a biologically inspired at-scale robotic insect," *IEEE Transactions on Robotics* **24**(2): 341-347 (2008).